Nanoparticle generation inside Ag-doped LBG glass by femtosecond laser irradiation

Marie Vangheluwe, Yannick Petit, Nicolas Marquestaut, Alexia Corcoran, Evelyne Fargin, Réal Vallée, Thierry Cardinal, Lionel Canioni

Nanoparticle generation inside Ag-doped LBG glass by femtosecond laser irradiation

Marie Vangheluwe,[1,2] Yannick Petit,[1,3,*] Nicolas Marquestaut,[1] Alexia Corcoran,[2,3] Evelyne Fargin,[3] Réal Vallée,[2] Thierry Cardinal,[3] and Lionel Canioni[1]

[1] *Centre Lasers Intenses et Applications– UMR 5107, Université Bordeaux I, 351 cours de la Libération, F-33405 Talence Cedex, France*

[2] *Centre d'Optique, Photonique et Laser – Université Laval, 2375 rue de la Terrasse, G1V 0A6 Québec, Qc, Canada*

[3] *Institut de Chimie de la Matière Condensée de Bordeaux – UPR 9048 CNRS, Chateau Brivazac, Avenue du Dr. Schweitzer, 33608 Pessac Cedex, France*

**yannick.petit@u-bordeaux.fr*

Abstract: Precipitation of silver nanoparticles (Ag-NPs) can occur in a silver-doped lanthanum borogermanate glass matrix, either under thermal annealing or femtosecond direct laser writing (DLW). Macroscopic transmission and localized μ-fluorescence emission spectra provide typical plasmon resonance behavior of Ag-NPs. Annealing leads to the spatially random homogeneous creation of small NPs at low concentrations, while DLW shows higher and broader plasmon peaks, proving highly concentrated 3D localized structured NPs. DLW at high fluencies shows photo-induced dichroism, potentially giving access to 3D dichroic photonic responses.

OCIS codes: (140.3390) Laser materials processing; (140.3450) Laser-induced chemistry; (160.2540) Fluorescent and luminescent materials; (220.4240) Nanostructure fabrication; (260.0260) Resonance; (300.1030) Absorption.

References

1. K. M. Davis, K. Miura, N. Sugimoto, and K. Hirao, "Writing waveguides in glass with a femtosecond laser," Opt. Lett. **21**(21), 1729–1731 (1996).
2. A. Royon, Y. Petit, G. Papon, M. C. Richardson, and L. Canioni, "Femtosecond laser induced photochemistry in materials tailored with photosensitive agents [Invited]," Opt. Mater. Express **5**, 887 (2011).
3. J. D. Musgraves, K. Richardson, and H. Jain, "Laser-induced structural modification, its mechanisms, and applications in glassy optical materials," Opt. Mater. Express **1**(5), 921 (2011).
4. M. Bellec, A. Royon, B. Bousquet, K. Bourhis, M. Treguer, T. Cardinal, M. Richardson, and L. Canioni, "Beat the diffraction limit in 3D direct laser writing in photosensitive glass," Opt. Express **17**(12), 10304–10318 (2009).
5. J. Sancho-Parramon, V. Janicki, P. Dubcek, M. Karlusic, D. Gracin, M. Jaksic, S. Bernstorff, D. Meljanac, and K. Juraic, "Optical and structural properties of silver nanoparticles in glass matrix formed by thermal annealing of field assisted film dissolution," Opt. Mater. **32**(4), 510–514 (2010).
6. J. Qiu, M. Shirai, T. Nakaya, J. Si, X. Jiang, C. Zhu, and K. Hirao, "Space selective precipitation of metal nanoparticles inside glasses," Appl. Phys. Lett. **81**(16), 3040 (2002).
7. J. Qiu, X. Jiang, C. Zhu, M. Shirai, J. Si, N. Jiang, and K. Hirao, "Manipulation of gold nanoparticles inside transparent materials," Angew. Chem. Int. Ed. Engl. **43**(17), 2230–2234 (2004).
8. Y. Shimotsuma, K. Hirao, J. Qiu, and K. Miura, "Nanofabrication in transparent materials with a femtosecond pulse laser," J. Non-Cryst. Solids **352**(6-7), 646–656 (2006).
9. J. Qiu, K. Miura, and K. Hirao, "Femtosecond laser-induced microfeatures in glasses and their applications," J. Non-Cryst. Solids **354**(12-13), 1100–1111 (2008).
10. Y. Dai, G. Yu, M. He, H. Ma, X. Yan, and G. Ma, "High repetition rate femtosecond laser irradiation-induced elements redistribution en Ag-doped glass," Appl. Phys. Lett. B **103**(3), 663–667 (2011).
11. N. Marquestaut, Y. Petit, A. Royon, P. Mounaix, T. Cardinal, and L. Canioni, "Three-dimensional silver nanoparticle formation using femtosecond laser irradiation in phosphate glasses: analogy with photography," Adv. Funct. Mater. **24**(37), 5824–5832 (2014).
12. A. Podlipensky, A. Abdolvand, G. Seifert, and H. Graener, "Femtosecond laser assisted production of dichroitic 3D structures in composite glass containing Ag nanoparticles," Appl. Phys., A Mater. Sci. Process. **80**(8), 1647–1652 (2005).

#254955 Received 2 Dec 2015; revised 23 Jan 2016; accepted 1 Feb 2016; published 9 Feb 2016

13. A. Stalmashonak, G. Seifert, and H. Graener, "Optical 3D Shape Analysis of Metallic Nanoparticles after Laser Induced Deformation," Opt. Lett. **32**, 3215 (2007).
14. P. Zijlster, J. W. M. Chon, and M. Gu, "Five-dimensional optical recording mediated by surface plasmons in gold nanorods," Nature Letters **459**, 08053 (2009).
15. P. Gupta, H. Jain, D. Williams, O. Kanert, and R. Kuechler, "Structural evolution of $LaBGeO_5$ transparent ferroelectric nano-composites," J. Non-Cryst. Solids **349**, 291–298 (2004).
16. Y. Takahashi, K. Kitamura, Y. Benino, T. Fujiwara, and T. Komatsu, "LaBGeO5 single crystals in glass and second-harmonic generation," Mater. Sci. Eng. B **120**(1-3), 155–160 (2005).
17. V. N. Sigaev, E. A. Alieva, S. V. Lotarev, N. M. Leppekhin, Y. S. Priseko, and A. V. Rasstanaev, "Local crystallization of glasses in the La_2O_3-B_2O_3-GeO_2 system under laser irradiation," Glass Phys. Chem. **35**(1), 13 (2009).
18. A. Stone, M. Sakakura, Y. Shimotsuma, G. Stone, P. Gupta, K. Miura, K. Hirao, V. Dierolf, and H. Jain, "Directionally controlled 3D ferroelectric single crystal growth in $LaBGeO_5$ glass by femtosecond laser irradiation," Opt. Express **17**(25), 23284–23289 (2009).

1. Introduction

Significant progress in advanced functionalized materials was achieved during the last two decades. Space-selective three-dimensionally (3D) structured composite materials with enlarged optical properties [1–3] were developed using direct laser writing (DLW) and thermal processes successively or simultaneously in tailored glass matrices.

Metal ion glass doping also had a huge impact since it can lead to the formation of metallic nanoparticles (NPs), either spatially randomly-distributed from thermal annealing [4, 5] or from laser-induced 3D space-selective precipitation [6–11], leading to plasmonic properties thanks to surface plasmon resonances. Additionally, with metal-glassy composite materials, DLW led to the realization of dichroic structures related to laser-induced aspherical silver NPs [12, 13] in silicate after the ion exchange process. It enables the demonstration of true five-dimensional optical recording by taking advantage of the wavelength-dependent anisotropic plasmon response of poly-disperse silver rods [14]. Silicate glass matrices often suffer from a very low solubility of the silver ions and also a low refractive index. Weak plasmon resonance magnitude can thus be achieved in bulk silicate glasses. A lanthanum boro-germanate matrix is of interest because it combines good solubility of the silver ions, high refractive index and good optical quality as previously reported [15–17].

In this article, we report what would be, to our knowledge, the first study of the incorporation of silver ions in the LGB glass. We focused on the precipitation of NPs, from both thermal and laser-induced methods, providing a detailed comparative analysis, especially about the strength of the associated effective absorption properties. The consequence of NP precipitation on fluorescence was also studied, giving a direct experimental access to local laser-induced absorption. Finally, an unexpected anisotropic transmission behavior was also observed. All these aspects make the LBG matrix a good candidate for silver-ion doping supporting its high potential for the development of photonic devices.

2. Materials and methods

Glass samples with the composition 99 [$25La_2O_3$ – $25B_2O_3$ – $50GeO_2$] + 1 Ag_2O (mol %) were made using the melt-quenching technique. The raw material mixture was placed in a Pt crucible and melted up to 1250 °C for 10 hours. The obtained glass samples were annealed at 25°C below the glass transition temperature T_g = 687 ± 3°C for 15 hours and cut (1 mm thick), and optically polished. These pristine glass samples were homogeneous, colorless and transparent (Fig. 1(a)).

The pristine glass samples were annealed close to their glass transition temperature at 680°C for 2 hours, leading to spatially randomly homogeneous silver NP precipitation after thermal treatment. Laser-induced irradiation was conducted using a regenerative amplified Ti: Sapphire laser (RegA 9000, Coherent Inc. at 800 nm, pulse duration $\tau =$ 80 fs, and repetition rate $f_{rep} = 250\,\text{kHz}$). The beam was tightly focused in the bulk at a constant depth of 180 μm (objective, 40 ×, N.A.= 0.65). The focal spot diameter was estimated to $2 \times \omega_0 =$ 0.9 μm.

#254955 Received 2 Dec 2015; revised 23 Jan 2016; accepted 1 Feb 2016; published 9 Feb 2016

The samples were mounted on a high-resolution motorized 3D translation stage. The selected irradiation pattern was defined as 1 mm^2 (Fig. 1(c)), consisting of individual lines equally separated by a spacing of 10 µm. The chosen writing speeds ($v = 250$ and 750 µm/s) led to the estimation of the number of pulses N that overlapped at each position during laser structuring at constant translation speed, as $N = 2 \times \omega_o \times f_{rep} / v$. The average power (P = 125 and 230 mW measured after the objective lens), was adjusted by a half-wave plate and a polarizer. The pulse fluence was estimated as $F = P / (f_{rep}(\pi \times \omega_o^2))$.

The annealed sample was ground into powder and the embedded silver nanoparticles were observed using a transmitted electron microscope (TEM, TECNAI F20). For pristine and processed samples (both annealed or irradiated samples), the absorption spectra were measured by a UV/Vis spectrophotometer (Varian Cary 5000). A micro-fluorescence study was performed with a confocal µ-spectrometer (Horiba Jobin-Yvon, LabRAM HR800), with a reflective microscope objective (UV enhanced Cassegrain objective, 36 ×, N.A. = 0.5, typically leading to a micron-scale lateral spot size. The excitation source was a CW He: Cd laser (Kimmon, 325 nm, 30 mW, TEM_{00}).

3. Results and discussion

After heat treatment, the annealed sample became yellow (Fig. 1(b)). The TEM images (Fig. 1(d)) revealed the presence of spherical NPs of 6.6 ± 3.5 nm diameter, estimated from the particle histogram over a set of 23 particles (Fig. 1(e)). However, we should note that this method of observation does not allow us to visualize nanoparticles of very small size.

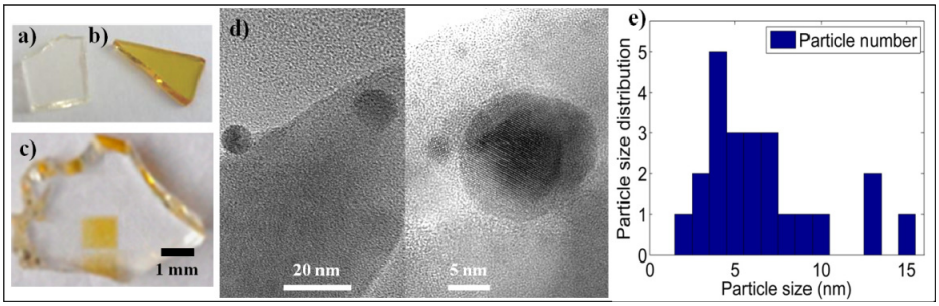

Fig. 1. Samples of the Ag -doped LBG glass **(a)** before and **(b)** after annealing at 680 °C for 2h, and **(c)** after localized femtosecond laser irradiation with the irradiation parameters: N = 900 with F = 39 J/cm^2 (transparent square of 1 mm^2) and 72 J/cm^2 (green square). **(d)** TEM image of silver nanoparticles inside LBG-Ag glass after annealing at 680 °C for 2h and **(e)** measured particle size distribution.

In the case of the annealed sample, the absorbance spectrum (Fig. 2(a), spectrum β) showed a relatively narrow Lorentz-shape absorption band centered at 449 nm (FWHM = 35 nm), associated to the extinction due to the Ag-NPs surface plasmon resonance. Laser irradiations on pristine glass sample led to plasmon resonance also located near 445 nm. A broader Gaussian-shape absorption band (FWHM = 92 nm), as seen in Fig. 2(a), suggests the production of Ag-NPs with a larger size distribution, a spatial gradient of NP concentration distribution and local dielectric constant modifications. For weak irradiation conditions (e.g. F = 39 J/cm^2 and N = 900, Fig. 3(a), spectrum γ), absorbance spectra did not show evidence of the plasmon band, which does not necessarily mean the absence of NPs. As the laser fluence increases (e.g. F = 72 J/cm^2), the plasmon band appears and grows with the increase (from N = 300 to 900, Fig. 2(a), spectra δ and ε) of the number of pulses.

In the case of the homogeneous samples (the pristine and annealed ones), the calculation of the linear absorption coefficient was performed with respect to the actual sample thickness (typically 1 mm). This led to low absorption coefficients (Fig. 2(b), spectrum β), related to

#254955 Received 2 Dec 2015; revised 23 Jan 2016; accepted 1 Feb 2016; published 9 Feb 2016

rather low spatial densities of NPs. In the case of laser-modified samples, the samples were first cut and polished perpendicularly to the written lines. Thus, the resulting longitudinal cross-sections of the structured areas gave a direct visual access to their thicknesses, as well as to the nature of the photo-induced modification, either in terms of index profile change or of the precise localization of the NPs. Indeed, laser-modified volumes (Figs. 1(c) and 3(c)) showed darkened profiles with restricted thickness (typically 10 µm measured for both spectra δ and ε of Fig. 2(b)) but containing very high NP concentrations, which led to extremely high absorption coefficients, typically up to 1200 cm^{-1}. Moreover, by considering the lateral distance between two successive darkened areas containing NPs and the associated fractional coverage of the sample section, one can claim that such absorption coefficients may locally be even higher. Therefore, such NP densities correspond to an effective medium, requiring the Maxwell-Garnett theory that we used to calculate the filling factors and mean radius of the Ag-NPs [12]. Such filling factors from DLW are two orders of magnitude higher than that obtained with annealing (typically from 10^{-6} up to 10^{-4}).

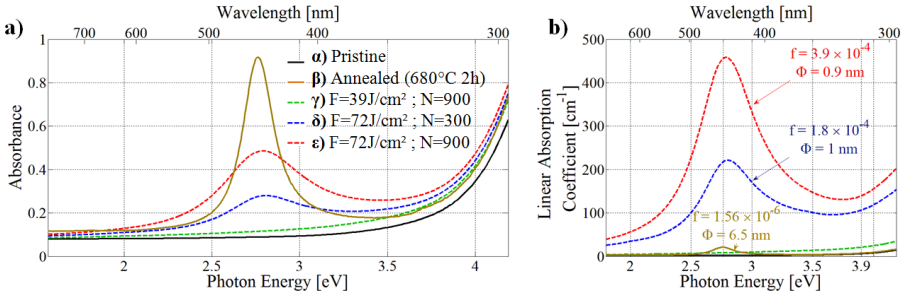

Fig. 2. (a) Absorbance spectra of the 1mm thick Ag^+-doped LBG glass samples: (α) pristine sample, (β) annealed sample, (γ, δ, ε) irradiated samples for three irradiation conditions, respectively. **(b)** Linear absorption coefficient spectra of the Ag^+-doped LBG glass samples for the five (α, β γ, δ, ε) samples, as computed with respect to the actual thickness of the exposed region. f and ϕ are the filling factors and mean radius of the Ag-NPs, estimated from the Maxwell-Garnett theory for silver NPs in the LGB glass.

Complementary information was provided by a fluorescence emission study of the samples. The pristine glass (Fig. 3(a), spectrum α) showed a strong intrinsic fluorescence emission, centered at 525 nm which is associated to pre-existing emitting centers. According to our fluorescence excitation and emission, the pristine glass would contain paired silver ions as well as another group of species, that we call Ag_α, responsible here for our fluorescence spectrum. The fluorescence spectrum ratio between the normalized spectral response of the pristine glass (Fig. 3(a), spectrum α) and the weak irradiation condition (F = 39 J/cm^2 and N = 900, Fig. 3(a), spectrum γ) was roughly equal to 1. This lack of spectral modification means that no evidence of a nanoparticle plasmon influence is observed and no silver clusters are created after DLW. The Ag_α elements would thus be stable and at equilibrium in the glass material. On the other hand, the fluorescence amplitudes of the different DLW conditions are almost the same (Fig. 3(a), spectra γ, δ and ε), but larger than the amplitude for the pristine (Fig. 3(c), fluorescence image**)**. One can suppose that the geometric shape of the structures (Fig. 3(c), bright-field image**)** and the associated index changes play the role of a lens to enhance the fluorescence excitation and/or collection inside the structure. Furthermore, the fluorescence spectra corresponding to larger irradiation (profiles δ and ε) are significantly modified in the 420-470 nm range, namely the spectral region of the Ag-NPs surface plasmon resonance. The Fig. 3(b) shows the fluorescence spectrum ratios between our new reference from weak irradiation condition spectrum γ and the high irradiation condition spectra δ and ε (Fig. 3(b), plain lines). These ratios show a Gaussian-shape band located near 445 nm directly related to the selected spectral absorption of the Ag_α fluorescence emission by the Ag-NPs. At low photon energy, the ratios equal 1 meaning that no fluorescence is absorbed since such

#254955 Received 2 Dec 2015; revised 23 Jan 2016; accepted 1 Feb 2016; published 9 Feb 2016

spectral range is located too far from the plasmon resonance. As already seen with the linear absorption coefficients (Figs. 2(b) and 3(b), dotted lines), while the laser fluence increased (e.g. F = 72 J/cm^2), the plasmon influence was shown to appear around the plasmon central wavelength (typically 445 nm) and to grow with the increase of the number of pulses (from N = 300 to 900, Figs. 3(b), spectra δ and ε). Here, the intrinsic glass fluorescence was used to identify the plasmon behavior, since the estimated fluorescence ratios (Fig. 3(b)) roughly correspond to the linear absorption coefficients obtained in Fig. 2(b) for spectra δ and ε, even though these two approaches differently integrated the local spatial distributions of NPs.

To describe the evolution of the silver species by DLW, we follow the mechanism previously introduced in Ref [11], where laser irradiation had shown the formation of silver species, labeled Ag_β, an intermediate state of silver clusters that had showed no specific fluorescence emission, but that appeared to be necessary for the subsequent NP formation. Here, the Ag-doped LBG pristine glass already contains a fraction of such silver clusters Ag_β, allowing for the growth of a small quantity of Ag-NPs during the annealing process (Figs. 1 and 2(a), spectrum α). During DLW, high local temperature can be reached, directly allowing thus for diffusion processes to grow such Ag_β species and reduce them into Ag_n NPs.

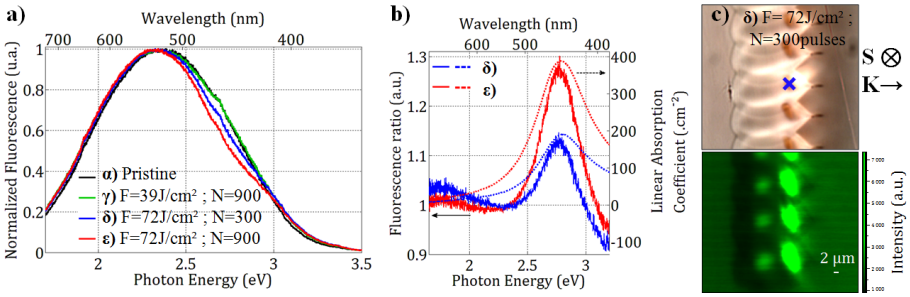

Fig. 3. Micro-fluorescence studies of the Ag^+-doped LBG glass excited at 325 nm versus irradiation parameters (the same as those of the absorbance study, Fig. 2). **(a)** Normalized fluorescence spectra measured at the position marked by the blue cross. **(b)** Associated fluorescence ratio spectra with weak irradiation condition γ, which highlights the fluorescence discrepancy due to NP plasmon extinction (full lines) and the linear absorption coefficients from Fig. 2(b). **(c)** Top image: transversal cross-sections of the structured area with the parameters (F = 72 J/cm^2 and N = 300 pulses); Top image from white light transmission microscope imaging; Bottom image is the reconstructed fluorescence image, showing the fluorescent silver cluster spatial distribution. Note $\vec{S}$ is the axis of the laser displacement inside the bulk during laser structuring, and $\vec{K}$ is the associated laser propagation direction.

Finally, we explored broadened irradiation conditions in terms of higher fluence, but lower number of pulses, which turned out to bring new fundamental observations thanks to macroscopic transmission measurements in polarized light. For F = 79 J.cm^{-2} and N = 112, the resulting linear absorption coefficient led to a broad band centered at 454 nm, corresponding to the plasmon response of the laser-induced NPs. No significant influence of the incident linearly polarized light was observed, globally associated to an isotropic optical response (Fig. 4, spectra ζ, for horizontal (H = parallel to the lines) or vertical (V = perpendicular to the lines) polarizations, as well as for larger number of pulses (Fig. 4, spectra η, F = 79 J.cm^{-2} and N = 450, for H, V or at 45° polarizations). The higher number of pulses finally led to the appearance of two bands located at even higher but polarization-dependent absorption coefficients (Fig. 4, spectra θ, F = 102 J.cm^{-2} and N = 450, for H, V or at 45° polarizations). The interpretation of such optical anisotropy is still under investigation. The origin may result from the laser-induced creation of oriented non-spherical oblate NPs (in addition to the spherical ones), corresponding to the second absorption band at 488 nm [13]. Since we wrote linear patterns, we also noticed diffraction grating effects whose efficiency

#254955 Received 2 Dec 2015; revised 23 Jan 2016; accepted 1 Feb 2016; published 9 Feb 2016

may be polarization-dependent. In such case, the diffraction phenomenon may also contribute to the extinction behavior, leading to an effective anisotropic response.

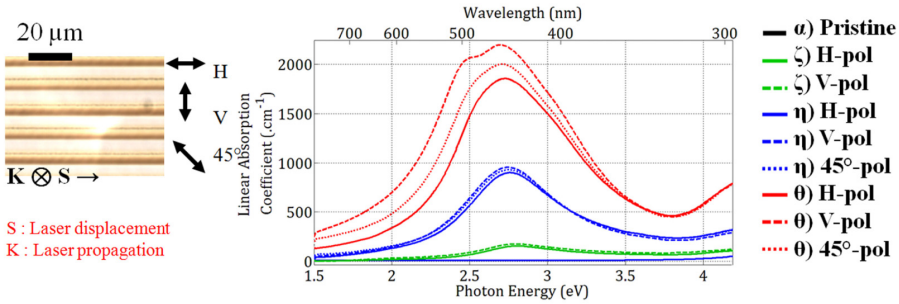

Fig. 4. Linear absorption spectra of the Ag^{+} -doped LBG glass in polarized light, for the pristine glass (spectrum α), and for three other irradiation conditions: spectra (ξ) for F = 79 J.cm^{-2} and N = 112, (η) F = 79 J.cm^{-2} and N = 450, and (θ) F = 102 J.cm^{-2} and N = 450, respectively, in structured areas (see insert) for H, V and 45° linear polarization direction.

4. Conclusion & perspectives

In this article, we have reported for the first time, the silver ion insertion in the well-known LBG glassy matrix. Besides the localized dielectric phase transition by means of either thermal annealing or of laser irradiation [18] we have proposed that such silver-doped glassy matrix can also undergo metallic Ag-NP precipitation, also either under thermal annealing or under DLW. Similarly to the localized dielectric phase transition, thermal annealing has led to the spatially random homogeneous creation of small NPs (6.6 ± 3.5nm) at rather low concentrations, while femtosecond DLW at room temperature has produced 3D spatially-localized high-concentration areas of NPs. This demonstrated that the LBG matrix provides a very favorable environment for NP precipitation and stabilization.

NP formation was tracked with macroscopic transmission measurements, but also by localized µ-fluorescence emission. We have recorded the plasmon resonance behavior, centered at 445 nm, which could be associated to an extremely high linear absorption coefficient, over 1000 cm^{-1}. In particular, such coefficients were locally much higher (by 3 orders of magnitude) in the region of laser-induced modifications, compared to that obtained with the annealing process. Finally, for very high fluencies, DLW even led to a polarization-dependent absorption behavior including the isotropic plasmon band at 445 nm, and a new band centered at 500 nm for the probing polarization parallel to the laser-induced lines, which may open dichroic polarization-dependent optical responses.

Finally, by exploring lower fluencies, localized moderate amount of NPs could be regarded as potential nucleation centers for localized dielectric phase transitions, while considering a supplementary nucleation treatment. Therefore, the silver-doped LBG glass could become a relevant candidate for plasmonic functionalities, resulting from the multi-scale laser-induced 3D architecture including both spatial distributions of metallic NPs and non-centrosymmetric dielectric crystallites. This suggests potentialities for the enhancement of the nonlinear optical behavior of dielectric particles in interaction with the NPs.

Acknowledgment

This research was supported by the French Agency of National Research, the French Aquitaine Region, the Cluster of Excellence LAPHIA (ANR-10-IDEX-03-02), the Canada Foundation for Innovation (CFI), the Natural Sciences and Engineering Research Council of Canada (NSERC), and the Fonds de Recherche du Québec-Nature et Technologies (FRQNT).